ORNL/SPR-2023/2892

FY23 ARPA-E Milestone Report
Corrosion Testing Trade Study on Testing Methods in Molten Salts

Approved for public release.
Distribution is unlimited.

E. Kiosidou
D. Sulejmanovic
B. A. Pint

March 2023

OAK RIDGE NATIONAL LABORATORY
MANAGED BY UT-BATTELLE FOR THE US DEPARTMENT OF ENERGY

FY23 ARPA-E Milestone Report:
Corrosion Testing Trade Study on Testing Methods in Molten Salts

E. Kiosidou, D. Sulejmanovic and B. A. Pint
Materials Science and Technology Division, Oak Ridge National Laboratory

Summary
In assessing molten salt compatibility with structural materials, static testing is often reported because it is easy to conduct. However, in order to assess mass transfer, where material dissolves in the salt in the hot section and may precipitate out of the liquid in colder regions, a flowing salt experiment in a temperature gradient is needed. While a forced convection or pumped loop produces prototypic flowing conditions, it also is a multi-million dollar investment. Among the less expensive dynamic testing options, the thermal convection loop (TCL) was favored during the 1960's development of molten salt reactor technology. Because the workforce and core facilities are currently available to conduct TCL experiments, it is the least expensive strategy to evaluate candidate structural alloys in flowing molten salt conditions.

1. Introduction

Due to their favorable thermochemical and thermophysical properties, molten salts are considered for thermal energy storage applications and advanced nuclear reactors as both coolants and fuels. The unique properties of molten salts make them an attractive option for advanced nuclear reactors, as they can operate at high temperature and low pressures which reduces the risk of reactor accidents. Molten salts are composed of group I and II cations, such as Li^+, Na^+, K^+, Be^{2+}, Mg^{2+}, and halide anions, such as F^-, Cl^-. Some of the most commonly studied salt mixtures for molten salt reactor (MSR) applications are NaCl-$MgCl_2$, FLiNaK (LiF-NaF-KF) and FLiBe (LiF-BeF_2).

Another prominent application of molten salts is in thermal energy storage systems, namely concentrating solar power. Molten salts have a high heat capacity, which allows them to store large amounts of thermal energy. Mirrors in concentrating solar plants produce enough thermal energy to melt the salts which can then be used to power steam turbines to generate electricity during the day and at night. Nitrate salts ($LiNO_3$ and $NaNO_3$) have been used in concentrating solar power plants over the last several decades. In addition to nitrate salts, chloride salt mixtures, such as NaCl-KCl-$MgCl_2$, are also being investigated due to their greater thermal stability.

Despite their promising use case, molten salts are still not widely used for thermal energy storage or MSR applications. One of the main reasons for this is the corrosive nature of molten salts. Molten salts can cause a range of corrosion-related problems, such as mass transfer and metal dissolution, which can degrade material performance. Molten salts can be highly corrosive to certain materials, which can limit the options for materials selection for salt-facing components. The increased cost associated with the use of compatible Ni-based materials and the inherent corrosive nature of molten salts has limited their widespread commercialization.

Materials compatibility with molten salts is a crucial consideration in the design, construction, and operation of systems involving the use of molten salts. For this reason, compatibility testing of materials in molten salt environments is an important first step in the qualification of materials.

Historically, compatibility testing of materials in liquid environments can be classified into two general areas: static and dynamic or flowing experiments. In static tests, the molten salt is in contact with the test material and the exposure is conducted at a constant temperature for a specified time. These tests are frequently performed because they are relatively easy to conduct. However, while they can quantify dissolution and reaction product formation, they cannot be used to study mass transfer, which is a major concern with working fluids. In a temperature gradient, dissolved material from the hot side can precipitate out of the liquid as it cools and the solubility decreases. Thus, in order to study mass transfer, flowing tests are needed which allow the salt to flow in a temperature gradient, usually with a constant flow rate for a fixed time period. The report will briefly review static testing and then focus on the different types of flowing salt experiments that might be conducted and their pros and cons.

2. Static molten salt tests

While the focus of this report is on flowing salt corrosion tests, the static compatibility testing in molten salts is still very useful as it can provide baseline results that can be informative for subsequent flowing salt tests. Prior to performing flowing salt compatibility tests, understanding the extent of corrosion from a static test can be very useful in terms of risk assessment, screening of alloys and performing targeted corrosion experiments to investigate specific variables such as impurity additions. Typically, the static corrosion tests are done in an inert environment such as gloveboxes or in welded capsules or sealed containers. Each method has its advantages and disadvantages. The glovebox test is usually the quickest and simplest test as it only requires a crucible, test specimens, salt and a furnace inside a glovebox. This type of experiment also enables in situ electrochemical salt monitoring. However, impurities in the argon may be gettered by the salt and increase impurities during the duration of the exposure.

Welded or sealed capsule tests are somewhat more complicated than the glovebox tests because of the need to seal the capsules by either welding or other gas-tight sealing methods. The welded capsule experiments used at Oak Ridge National Laboratory (ORNL) are shown in Figure 1. The

Figure 1. (a) schematic of ORNL welded capsule experiment using parts shown in (b) including graphite spacer to prevent interaction between the inner Mo capsule and outer SS capsule; (c) capsules in a box furnace for exposure.

advantage of welded capsules which include inner and outer capsules is that there is a low chance of impurity ingress during the test. Crucible tests without welding (e.g. conducted in a bolted shut vessel placed into a furnace) are sometimes done outside the glovebox but with an argon cover gas which has a similar contamination risk as a glovebox. If the seal fails on a crucible test, the salt might become contaminated.

Pre- and post-exposure characterization after static exposures includes (1) mass change, (2) metallographic sectioning of the specimens to determine the depth of attack, (3) salt chemistry changes and (4) electrochemical assessments of the salt. Mass change alone can be misleading. Microstructure characterization provides a better assessment of the attack observed. Salt chemistry measurements provide a check on which elements are dissolving and may identify reactions due to the choice of container. Electrochemistry is useful in understanding the reactions observed. All of these strategies carry over to flowing experiments.

3. Flowing molten salt tests

To better represent the flowing salt conditions in a MSR or thermal storage application, dynamic tests in flowing salts are typically conducted, including a temperature gradient. These tests have included simple rocking ('seesaw') or spinning tests [Vreeland 1953]. To avoid the use of pumps and valves but achieve more uniform flow, thermal convection loops (TCLs) [Koger 1973, 1974, Keiser 1979, Raiman 2022, Pint 2019, 2022, Kelleher 2022] have been used since the 1950's at ORNL [Vreeland 1953]. To achieve more prototypic conditions, a pumped or forced convection loop (FCL) is the natural progression in testing. Many different methodologies were explored at ORNL during the 1950's Aircraft Reactor Experiment (ARE) program and the 1960's Molten Salt Reactor Experiment (MSRE). However, TCLs became the predominant test methodology by the end of the MSRE program. For example, seesaw tests are mentioned by Richardson [1952] but Adamson [1961] only mentions TCL testing. The TCL strategy carried over into liquid metal evaluations for fission and fusion applications through to the present. The following sections discuss these various dynamic experiments and some of their advantages and disadvantages in terms of materials compatibility assessment.

3.1 Stirring or spinning tests

Perhaps the most basic dynamic test is to stir or spin the liquid and examples of these experiments can be found in a few references. Kondo et al. [2010] conducted a stirring test exposing Fe-9Cr-2W steel (designated JLF-1) to FLiNaK salt at 600°C. The salt was stirred in a pot using an impeller for 250 h and less mass loss was measured compared to a static experiment. However, the static experiment used only a small amount of salt (5 g) and the ratio of salt volume (V) to specimen surface area (SA) was not held constant and the V/SA ratio can have a strong effect on the amount of dissolution [Pint 2023].

Vreeland [1953] mentioned a spinning test for increasing the salt velocity. However, no data were included in that report. Higher velocities were achieved in 'whirligig' test developed at NACA in Cleveland (predecessor of NASA Glenn Research Center) [Desmon 1951, Vreeland 1953]. In the whirligig test, the salt circulated at velocities up to 762 cm/s (faster than a FCL at ~300 cm/s) [Kroger 1972e]. The whirligig test did not require pumps, valves or flow meters and the test loop

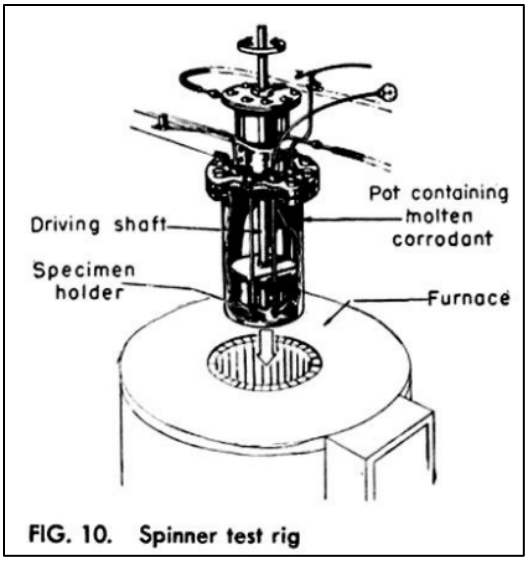

Figure 2. Spinner test from Vreeland et al. [1953]

was made from the material being evaluated to eliminate dissimilar material effects [Desmon 1951]. However, the attack was similar or only slightly increased compared to static tests [Briant 1953a, 1953b]. It was concluded that the high velocity resulted in a nearly isothermal test even when a temperature gradient was applied [Jordan 1955]. Also, the flow was not continuous. A comparison was reported between a whirligig test and a TCL using liquid Na exposed to Be specimens and Inconel 600 [Jordan 1955]. Similar corrosion trends were observed. The whirligig test did not appear to accelerate corrosion on samples that already had crevices [Briant 1953b]. A similar observation was made for seesaw tests discussed in the next section.

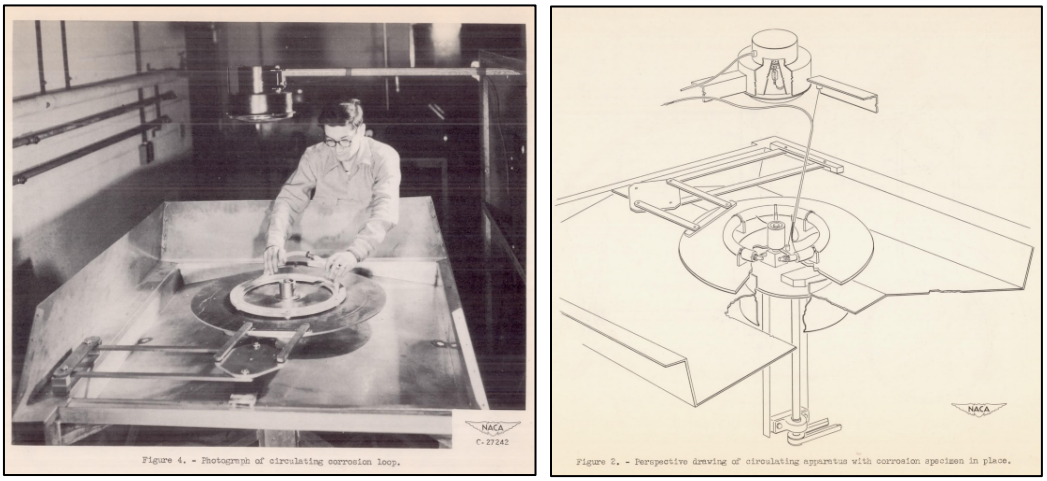

Figure 3. Whirligig setup demonstration and schematic from Desmon and Mosher [1951].

3.2 Seesaw or Rocker tests

Rocker tests are a type of dynamic molten salt materials compatibility experiments that utilizes the mechanical rocking of a furnace by about 20 degrees in order to move the liquid salt from one end of a tube or capsule to the other. One of the tube ends can be placed outside of the furnace to provide a temperature gradient between the two ends. The temperature differential can be adjusted based on the distance that the capsule extends out from the hot zone of the furnace. The rocking speed can typically be adjusted and this can be used as one of the variables during the rocker test.

A comparative study among seesaw, spinner and TCL tests was performed during the evaluation of liquid Na and NaK with BeO [Briant 1953b]. In terms of mass change, a ±1% variation was observed for the seesaw tests, up to 10% in the TCL and 71-100% mass loss in the spinner tests. The rotating velocity in the spinner test was ~20 cm/s, while the TCL was 3-5 cm/s. The increased velocity could induce a combined erosion-corrosion mechanism.

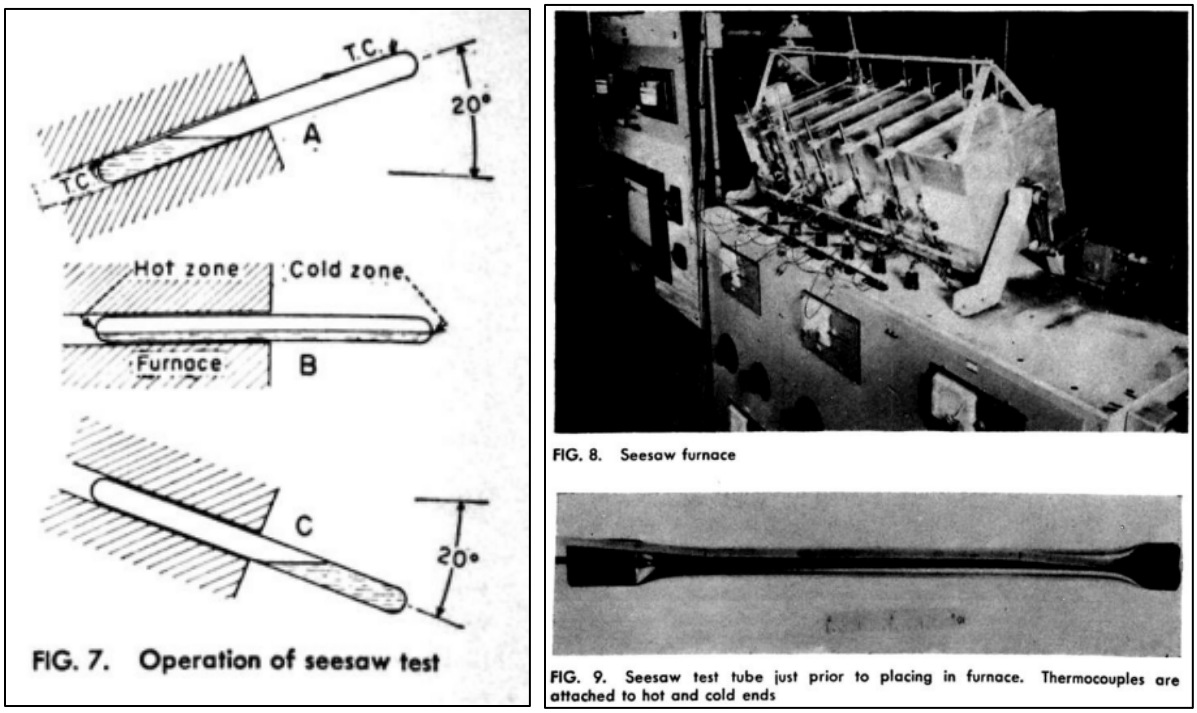

Figure 4. Seesaw test figures from Vreeland et al. [1953].

3.3 Thermosiphon

A thermosiphon is a natural convection dynamic test consisting of a crucible with heating on one end and flow channels for the hot cell to move up and then back down for further heating, Figure 5. Recent studies have been reported by Savannah River National Laboratory (SRNL) [Tavakoli Mehrabadi 2016, 2017] and the Kurchatov Institute [Ignatiev 2006, 2008, 2013]. Unfortunately, these studies converted results to electrochemical values such as current density and corrosion

potential which makes comparisons with other studies difficult. The SRNL thermosiphon made of Ni might cause a dissimilar material reaction and result in Cr and Fe in the salt reacting with the capsule walls possibly accelerating corrosion of the coupons shown in Figure 5 [Pint 2023]. Four coupons of the evaluated material (Haynes 230, Ni-22wt.%Cr-14W) were located in each zone and experiments were conducted in isothermal (static) and non-isothermal (dynamic) conditions. Temperature gradients of 600–850°C and 800–950°C were reported.

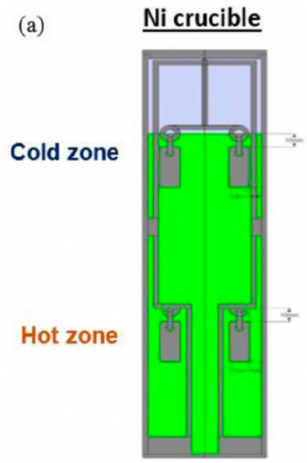

Figure 5. Schematic of thermosiphon with specimens hanging in the hot and cold zones as reported by Tavakoli Mehrabadi et al. [2016, 2017].

3.4 Thermal convection loops (TCL)

A TCL uses a temperature gradient between two parallel metallic sections to provide the driving force for natural salt circulation. The hot side is referred to as the hot leg (HL), and the cold side is called the cold leg (CL), with the temperature gradient typically in the range of 100°C between the two legs [Vreeland 1953, Raiman 2021, 2022]. TCL setups have varied in size from microloops (less than kg salt quantities) [Kelleher 2022] to larger installations from a few to several hundred kilograms [Keiser 1977, Raiman 2022]. Both chloride salts [Susskind 1960, Pint 2019, 2022a, Kelleher 2022] and fluoride salts [Koger 1972, 1973, 1974, Raiman 2022, Pint 2022b] have been evaluated in TCLs.

Depending on the size of the loop, the material being examined can either be the tubing itself [Kelleher 2022] or individual samples arranged in various locations along the HL and CL sections [Keiser 1977b, Pint 2019, 2022a, 2022b, Raiman 2022]. For the latter case, it was recommended that the examined samples be made of the same or similar alloy as the tubing to avoid galvanic corrosion between the two, which has been observed in the past between Inconel 600 tubing and 304 stainless steel (SS) samples [Koger 1970]. Longer duration experiments are typically suggested for a more accurate corrosion performance assessment. During a TCL experiment, the upper limit of the total duration depends on factors such as loss of power [Keiser 1977a, Kelleher 2022] or blockage of flow, particularly in the CL section of the loop due to deposit accumulation [Koger 1973, Kelleher 2022].

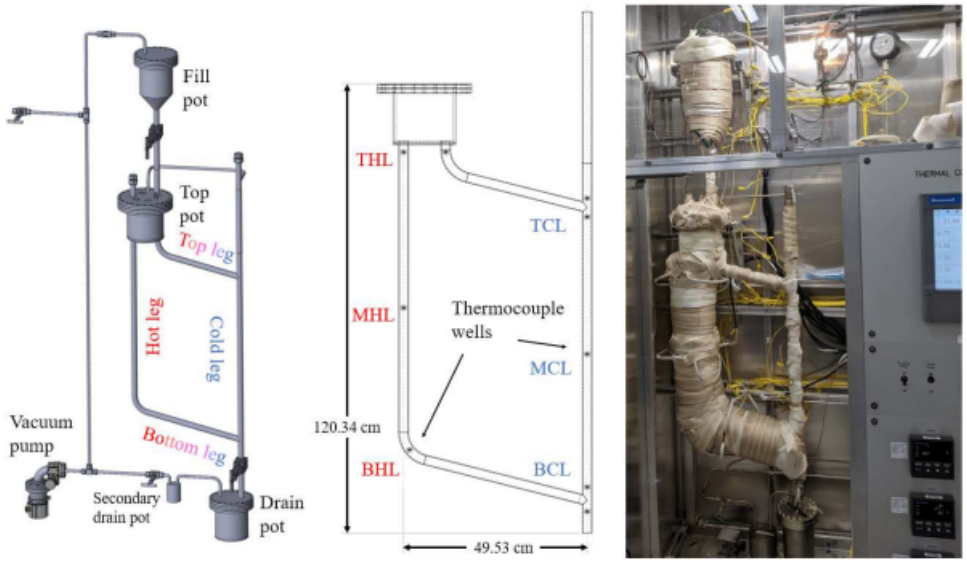

Figure 6. The current ORNL TCL design including a 3D rendering, 2D drawing and image during operation including the heaters and insulation. In the 2D drawing, thermowells are shown at the top (T), middle (M) and bottom (B) of the hot leg (HL) and cold leg (CL).

The general corrosion behavior observed during a TCL experiment is affected by parameters, such as salt purity, time, peak temperature and V/SA (Manly 1957; Raiman 2022; Sridharan 2013) or even the surface condition of the specimens [Susskind 1960]. The temperature gradient between the HL and CL creates conditions similar to a galvanic corrosion mechanism, where the HL exhibits dissolution and the CL exhibits deposition [Wang 2018]. Flow velocity has been shown to have a limited impact on corrosion, which makes TCL tests more attractive than FCLs (Manly et al. 1957; Britsch et al. 2019). The corrosion trends observed after a TCL run are characterized by deepest corrosion in the hottest part of the HL [Busby 2019] and highest deposition in the coldest part of the CL [Kelleher 2022, Koger 1974]. Often Cr dissolution is the primary corrosion mechanism discussed [Koger 1973] but more recent experiments have found Cr dissolution and Fe mass transfer [Raiman 2022, Pint 2022a]. Presumably, deposition in the CL occurs due to lower solubility [Raiman 2018]. No mass change is observed at the balance point, where the surface composition is in equilibrium with the salt [Koger 1973].

Various materials have been examined throughout the years as potential candidates for MSR applications in both chloride and fluoride based molten salts using a TCL. A recent study [Kelleher 2022] proposed a microloop, which allowed performance of multiple experiments for multiple materials in chloride based molten salts, i.e. NaCl-$MgCl_2$ and $MgCl_2$-NaCl-KCl. The examined alloys were: 316/316L, 316/316H, 600, N, 800H, 617, 625, C-276 and 200/201. It was found that Ni-based alloys C-276, Alloy 600 and Alloy N exhibited the smallest corrosion rates, being less than 100 µm/yr. These materials exhibited formation of a Mo-rich layer, of a labyrinth-type microstructure, on their surface, which acts protectively against thermal gradient mass transfer corrosion, since Mo is resistant against chloride attack.

It was also suggested that the ternary eutectic $MgCl_2$-NaCl-KCl salt can be used as a heat transfer salt, since it has a lower melting point than its binaries. Use of a purified salt is always recommended, in order to reliably rank the corrosion behavior of different materials in molten salts [Kelleher 2022]. The observed corrosion performance and proposed corrosion mechanisms of various materials during their exposure in flowing molten chloride salts, is presented below:

Stainless steels (SS) of the austenitic type were found to exhibit high susceptibility to corrosion in chloride molten salts [Kelleher 2022]. A network of voids was observed in the HL, which was Cr and Fe depleted, leaving areas rich in Ni and Mo. No corrosion or deposition was observed in the CL. Cr depletion did not progress along the grains, it remained uniform, in contrast to what is usually seen during static molten chloride salt tests [Kelleher 2022], and it has also been reported during other TCL tests in both binary LiCl-KCl and ternary NaCl-KCl-$MgCl_2$ (30-20-50 mol%) eutectic salts for an austenitic 347 SS (Susskind et al. 1960). Susskind et al. (1960) in the same study they observed transgranular corrosion for a martensitic 410 SS alloy in the HL region in both of these salts and a combination of intergranular and transgranular attack for a steel containing 2 ¼ Cr-1 Mo in the ternary eutectic salt. The uniform corrosion behavior reported by Kelleher et al. [2022] was observed for both purified and unpurified salt. In the latter case, the same corrosion effect required less time. A proposed corrosion mechanism is that Cr and Fe are converted to their chlorides upon exposure to the molten salt, leaving the metallic surface. The concentration gradient that results from that process forces more metallic elements to diffuse from the bulk of the material towards the surface, forming a new salt and, thus, sustaining the depletion cycle [Kelleher 2022].

Alloy (Inconel) 600 was found to show superior corrosion performance in NaCl-$MgCl_2$ and $MgCl_2$-NaCl-KCl molten salts, being suggested as a benchmarking material [Kelleher 2022]. The same alloy has also been found to exhibit very good corrosion characteristics in a commercial K-Mg-Na chloride salt [Pint 2019, 2022a], exhibiting good compatibility up to 700 ºC, which can be further improved with additions of Mg [Pint 2019]. Voids and tunnels were observed in the HL, not always along the grain boundaries (GBs). A possible mechanism that may lead to void formation could be a) pitting, if all voids are interconnected and linked to the surface or b) the Kirkendall effect, which describes metallic diffusion and vacancy precipitation, where the voids are not necessarily connected to the surface (Manly et al. 1957; Kelleher, Gagnon, and Mitchell 2022; Bakish and Kern 1960). For the latter case, preferential leaching of Cr precedes, introducing compositional gradients, which they subsequently initiate further Cr diffusion from the bulk material (Bakish and Kern 1960). Precipitation of corrosion products from the salt was observed in the CL, rich in Fe and Cr. Following Fe and Cr depletion, Ni is the next to be attacked by the chloride salt, even though it is highly resistant to attack in fluoride salts. Attack was generally less with purified salt [Kelleher 2022].

Alloy (Hastelloy) N was found to exhibit mediocre performance in chloride molten salts [Kelleher 2022]. Hastelloy N generally exhibits better performance in fluoride than chloride salts [Koger 1973, Kelleher 2022]. Yet performance was not very satisfactory even with purified chloride salts. Both intra- and intergranular attack were detected. Intergranular attack was more severe, due to the high depletion in Cr, Fe and Ni. A possible corrosion mechanism would be that selective depletion of Cr, Fe and Ni along the GBs leads to deep crevasses, separating the grains from one

another, hindering diffusion of these elements through the GBs. This is when intragranular diffusion takes over. This extensive depletion led to vacancies, creating a maze-like morphology, reach in Mo [Kelleher 2022].

Alloy 800H exhibited very high susceptibility to corrosion in chloride molten salts. A representative corrosion rate would be 920 μm/yr. The main corrosion mechanism was intergranular corrosion (IGC) in the HL, attributed mainly to Cr depletion [Kelleher 2022].

Alloy 617 was found to exhibit a non-consistent corrosion performance in molten chloride salts, but generally the performance was deemed unsatisfactory [Kelleher 2022]. The worst corrosion case included extensive crevice attack, probably related to and enhanced by inherent defects in the material. Intragranular attack prevailed compared to intergranular attack. Fe and Cr were attacked the most, followed by Ni and Co. Mo was the most resistant of all, creating a maze-like layer. A proposed corrosion mechanism would be that corrosion starts as IGC, until it becomes diffusion limited. This is when it shifts to intragranular attack. The most susceptible alloying elements "are selectively leached" out until a Mo-rich structure remains [Kelleher 2022].

Alloy 625 has been ranked among the materials with the higher corrosion rates (>100 μm/yr.) in molten chloride salts exhibiting a corrosion rate of 280 μm/yr [Kelleher 2022]. The corrosion attack exhibited a trilayered corrosion zone, starting from the one on the surface: a) a Mo-rich zone of the labyrinth type, b) a Ni-rich zone, c) a Cr-depleted zone without voids, d) main alloy matrix. Cr is the first element to undergo thermal gradient mass transport corrosion at the HL, followed by Ni and Fe. Nb is the element that gets attacked next. The Mo structure has a protective effect: a) it does not allow salt to ingress in the base metal that easily, b) it does not allow migration of the susceptible elements from the base metal to the surface [Kelleher 2022].

Alloy C-276 has exhibited satisfactory corrosion performance during thermal gradient mass transport corrosion in chloride molten salts, with a representative corrosion rate of 45 μm/yr [Kelleher 2022]. Uniform depletion of all alloying elements was observed but Mo, leaving a labyrinth-type Mo-rich layer behind. A similar Mo-rich layer is also found in static corrosion tests [Kelleher 2022].

Alloy 200/201 was found to be unsuitable for flowing tests. The material exhibited a purely dendritic structure. Pure Ni was found to severely corrode in thermal gradient mass transfer corrosion tests, in contrast to static tests [Kelleher 2022].

Chloride salts are generally more chemically aggressive than fluoride salts and for this reason, similar materials do not exhibit the same compatibility between the two salts [Kelleher 2022]. This is probably related to the fact that the difference between the Gibb's free of formation between the salt fluorides and metal fluorides is larger than the corresponding one in a chloride based molten salt (Williams, Toth, and Clarno 2006; Olson et al. 2009; Knosalla et al. 2020). For example, Ni is compatible with molten fluoride salts but incompatible with chloride salts. Mo and W are inert in molten chloride salts [Kelleher 2022]. The primary mode of corrosion in fluoride salt is intergranular corrosion, while in molten chloride salts is the first route, followed by intragranular attack [Kelleher 2022]. Fluoride salts have some toxicity related to fluoride ions and they exhibit volume shrinkage during phase transition. However, they have high thermal conductivity, high

specific heat and stable chemical properties under high temperature and irradiation (Ma et al. 2022). Chloride salts, on the other hand, have high corrosivity, it is difficult to determine their limit operating temperature, but they have good thermal stability and conductivity (Ma et al. 2022). It has been reported that fluoride salts exhibit the best heat-transfer characteristics, followed by fluoroborates and last by chlorides (Williams, Toth, and Clarno 2006). FLiNaK is considered to be one of the best candidates in this term (Williams, Toth, and Clarno 2006).

The corrosion performance of various materials in flowing fluoride containing salts has also been studied extensively. Among those, a study conducted by Koger et al. (1973) focused on Hastelloy N, Ti-modified Hastelloy N, 304L stainless steel (SS) and maraging steel in LiF-BeF_2 with varying amounts of UF_4, ThF_4, ZrF_4 (fuel salt –FS) and a mixture of $NaBF_4$-NaF (coolant salt - CS). For the former case, the summation of H_2O+O_2 impurities was less than 100 ppm, while for the latter case it was over 500 ppm, which led generally to higher measured corrosion rates and a uniform extensive oxidation, which even included Ni and Mo (Koger 1973). Mo oxidation (MoO_2) has also been reported by Yang et al. (2022) during exposure of GH3535 (Hastelloy N) in FLiBe salt with NiF_2 impurities and O_2 leakage, both at the HL and CL of a TCL setup operating at 660 ºC and 561 ºC, respectively. Addition of Be metal can act as a "scavenger" of impurities, reducing the overall corrosion of the alloy (Yang et al. 2022; Ignat'ev et al. 2006).

More particularly, regarding the performance and corrosion mechanisms of individual alloys in fluoride containing salts, the following observations can be made:

Hastelloy N (Ni-7Cr-16Mo-5Fe) has been reported to exhibit very good corrosion performance in fluoride molten salts (Ignatiev and Surenkov 2013; Manly et al. 1958; Koger 1974; Guo et al. 2018; Koger 1972a), even though long-term exposure for 9 years led to significant voids and depths of attack in the hot section of a TCL (Koger 1972d; Sridharan and Allen 2013). During examination in the FS described above, Ti-modified, no-Fe containing Hastelloy N exhibited smaller mass change than standard Hastelloy N (Koger 1973). In a similar study conducted by Keiser (1977), 1-3.4% Nb-modified Hastelloy N exhibited at least as good a corrosion performance as the standard Hastelloy N. Small additions (≤2%) of Nb or even Al in Hastelloy N have also been suggested as promising reinforcements for use in MSRs in other studies (Ignat'ev et al. 2006; Ignatiev and Surenkov 2013). Standard Hastelloy N exhibited a corrosion rate of around 1.52 μm/yr, followed by maraging steel at 13.97 μm/yr, and finally 304L SS with 27.94 μm/yr (Koger 1973).

The corrosion mechanism in Hastelloy N has been found to be controlled by solid state diffusion of Cr in the alloy (Keiser 1977; Koger 1973; DeVan and Evans III 1962; Ignatiev and Surenkov 2013; Manly et al. 1958). It was found that the corrosion rate, expressed as normalized mass change, increases linearly with the increase in the Cr content of the alloy (Keiser 1977). This is related to the following equation (Keiser, Manning, and Clausing 1976):

$$\Delta M = BC_o\sqrt{Dt} \qquad (1)$$

Where ΔM is the loss of Cr from the alloy matrix, B is a temperature-dependent constant, C_o is the initial concentration of Cr in the alloy, D is the diffusivity of Cr in the alloy and t is the exposure time.

On a microscopic level, the mode of attack was primarily IGC (Rosenthal, Briggs, and Haubenreich 1972; Koger 1972c), sometimes including presence of voids (Koger 1972c) and sometimes not (Koger 1973), caused by Cr depletion along the GBs, leading to enrichment with Fe (Koger 1973). Preferential attack can further progress after Cr to Fe and then Ni, while Mo is the most resistant of all (Koger 1974). Cr is usually oxidized through participation in reactions with salt impurities, such as HF, NiF_2 and FeF_2 (Keiser 1977; DeVan and Evans III 1962; Manly et al. 1957) or UF_4 in the case of a fuel salt (Koger 1974, 1972c). This is feasible due to the fact that impurities change the fluorine potential ($\overline{\Delta G}_{F_2}$) of the salt, e.g. in FLiNaK or FLiBe (Sohal et al. 2010). In the case of presence of fission products, such as tellurium, cracking has also been observed intergranularly (Keiser, Manning, and Clausing 1976), with most studies suggesting precipitation of tellurium along the GBs as the cause for cracking (Ignatiev and Surenkov 2013; McCoy and McNabb 1972; Huntley and Silverman 1976). Alloy Hastelloy N modified with 1% Al addition has been found to be the most resistant against tellurium induced intergranular cracking (Ignatiev et al. 2008).

The dissolved Cr creates stable fluoride salt crystals, such as Na_3CrF_6 in a molten $NaBF_4$-NaF-KBF_4 salt (Koger and Litman 1969), which can either be deposited on the CL of the loop as salt crystals per se or just as Cr metal (Koger and Litman 1969), or not deposit at all and remain in a salt form in the loop (Koger 1974). What will happen depends on the kinetic stage of the corrosion process (fast or steady-state) (Koger 1974) and the temperature of the CL (Koger and Litman 1969). The final mass gain in the CL is not entirely dependent on the temperature, which is the case for the mass loss in the HL (Koger 1974).

304L SS and Maraging steel corrosion mechanism is through selective attack (or selective removal) of Cr with void formation (Koger 1972a), similarly to the behavior of Inconel 600 in molten chloride salts. The maraging steel ranks between 304L SS (worst) and Hastelloy N (best) in FLiBe based fuel salts (Koger 1972a). Void formation is based on the Kirkendall effect (Bakish and Kern 1960; Koger 1973; Manly et al. 1957). More specifically, the attack of the alloy includes the following steps (Koger 1973): 1) Cr oxidizes on the surface, 2) Cr gets depleted on the surface, 3) Cr diffuses from the base metal towards the surface, following the concentration gradient, 4) the diffusion is mostly 1D and is based on creation of vacancies, that is why, as Cr diffuses towards the surface, it leaves vacancies behind, 5) the vacancies gather at GBs, impurities, areas of different orientations in the lattice etc. and, finally, 6) the voids agglomerate as time and temperature increase. The corrosion attack for austenitic SS progresses fast and can lead quickly to clogging of the CL (Manly et al. 1957).

316H SS corrosion behavior in FLiNaK showed again selective attack of Cr in the HL, followed by Fe, leaving a Ni-rich region behind (Raiman et al. 2022). In the CL, the deposited layer was mainly rich in Fe and low in Cr, and for the specimens with the highest temperature in the CL it also included Ni (Raiman et al. 2022). Type *316 SS* seems to be unsuitable for use with fully alkali-metal-based salts, such as FLiNaK, where clogging of the CL can happen quite fast, and maybe the KF component is the major contributor for that matter. Other types of fluoride salts, such as Zr-based fluorides could be better candidates for this material (Adamson, Crouse, and Manly 1959). Another option for use of 316 SS with molten salts, e.g. with FLiBe, could be addition of

Be metal, which has been found to decrease the corrosion rate of this alloy at 650 ºC, from 15 µm/yr to less than 2 µm/yr (Keiser, DeVan, and Lawrence 1979).

Alloy Inconel 601 was examined by Keiser (1977) in similar FS as the one used by Koger (1973) and it was found that it exhibited porosity and increased mass loss for the hottest specimen in the loop. Similar observations have also been made for variations of *Inconel (811E, 690, 601, 606, 600)* and it was found that the extent of attack was positively correlated to the total iron and chromium component of the alloy (Koger 1972a). Void formation has been reported as the primary corrosion attack observation in a number of studies performed by ORNL in TCL experiments with FLiBe, with and without UF_4/UF_4 additions, which have been summarized by Guo et al. (2018). The formed voids did not necessarily interconnect to the surface, suggesting the Kirkendall effect (Manly et al. 1957), similarly to the observations made above for stainless steels. Similar observation regarding non-interconnected voids has been made by Adamson et al. (1959), during examination of this alloy in KF-NaF-LiF-UF_4 (43.5-10.9-44.5-1.1 mole%) FS for 500h. Selective Cr attack was the primary corrosion mechanism and it led to a sharp increase of the maximum depth of attack for the first 250 h, followed by a linear increase of smaller slope for the rest of the examination period (Manly et al. 1957). The sharp increase during the first part of the test has been linked to fast kinetics related to the presence of impurities in the salt (Manly et al. 1958; Sridharan and Allen 2013), which can also have large effect on the type and depth of corrosion, maybe larger than the composition of the salt itself (Adamson, Crouse, and Manly 1959). The second part expresses a steady state rate linked to the processes being driven by the thermal gradient in the TCL (Busby et al. 2019; Manly et al. 1958), following consumption of most of the impurities (Keiser, DeVan, and Manning 1977). The slope of the linear part is proportional to the U-content of the FS (Williams et al. 2003). Cr release was also confirmed through Cr-rich deposits on the coldest part of the CL (Manly et al. 1957; Keiser 1977). This alloy was deemed unsuitable for use in a molten salt breeder reactor (Keiser 1977).

Croloy 9M alloy was examined in flowing $NaBF_4$-NaF-KBF_4 and it exhibited severe clogging of the cold leg after 1440 h (Koger 1974). The deposited layer consisted mainly of a “dark grey plug” which was composed of almost pure Fe dendritic crystals. This could be related to the fact that the equilibrium concentration of iron fluorides in the salt is smaller at the CL temperature, compared to their equilibrium concentration between the salt and the alloy at the HL temperature (Koger and Litman 1969). Some smaller green crystals were also observed which were mainly Cr and Fe fluorides (Koger and Litman 1969).

3.5 Pumped or forced convection loops (FCL)

TCL tests can be used to determine compatibility of a salt with particular alloys and the most promising ones then can be further examined in a forced convection loop (FCL), where simulation of actual reactor conditions is performed, except for the radiation component [Crowley 1963], thus providing a more sophisticated examination protocol [Huntley 1973]. An example FCL at ORNL is shown in Figure 7 which uses FLiNaK salt. A second FCL was built to study chloride salts [Robb 2019, 2020, 2022]. In many cases, the molten salt under examination might need to be characterized first in a particular loop, for determination of heat and mass transfer, as well as,

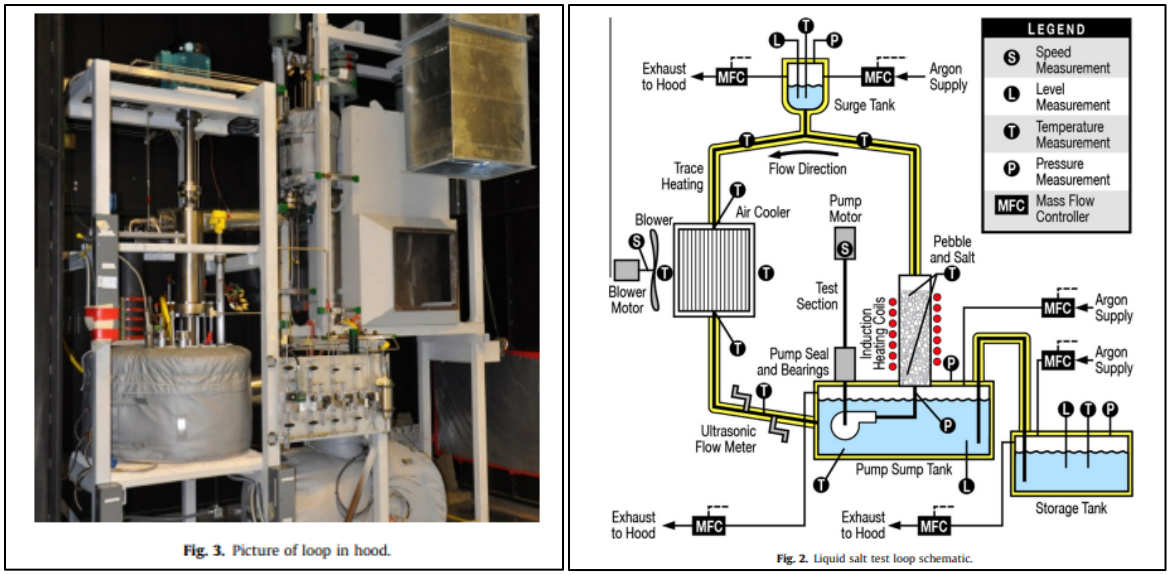

Figure 7. FLiNaK FCL from Yoder et al. [2010, 2014].

friction characteristics versus the applied Reynolds number [Cooke 1973, Silverman 1976,Ambrosek 2011]. Moreover, based on the selected molten salt type, flow rate and temperature, an appropriate pump, flow meter and pressure sensors can be selected (Sabharwall et al. 2010). FCL experiments could be considered more accurate in simulating the corrosion behavior of an alloy in an MSR, since they can attain high flow rates and sustain operational temperatures for longer (Nagasaka et al. 2008). However, it has been observed that flow velocity does not strongly affect the corrosion behavior, during the mass-transfer stage of corrosion [Koger 1972e, Keiser 1977, Manly 1957, Kelleher 2022]. Historically, the focus for FCL corrosion testing has been on Ni-based materials such as Inconel 600 and Hastelloy N [Crowley 1963, Huntley 1973].

Hastelloy N examination in fluoride based molten salts for 1-2.5 years revealed its superior performance compared to Inconel 600 [Crowley 1963]. Various studies performed at ORNL and summarized by Guo et al. [2018] also verify this observation. This is attributed to the smaller Cr content in Hastelloy N (7%) versus Inconel 600 (15%) [MacPherson 1960b], which is particularly vulnerable to IGC in fluoride salts, such as FLiNaK and FLiBe [Sohal 2010]. Similar observations were also made by Manly et al. [1958]. A summary of the superior performance of Hastelloy N versus Inconel and 316SS steel has been presented by Sridharan et al. (2008). Examination of 1%Nb-modified Hastelloy N in FCL experiments revealed similar or slightly improved corrosion performance compared to the standard Hastelloy N (Keiser 1977). A 2%Nb-modified Hastelloy N has been recommended for use in fuel salts of high velocity (Huntley and Silverman 1976). Finally, Ti-modified Hastelloy has also exhibited improved performance compared to the standard version (Koger 1972b). The corrosion attack mechanism was once again related to selective depletion of Cr [Crowley 1963, DeVan 1962], leaving behind a Mo-rich layer (MacPherson 1960a). This process proceeds initially fast as the impurities in the salt are being consumed and eventually it reaches a quasi-steady-state where the amount of Cr deposited on the cold part equals the amount

of Cr entering the circulation system (DeVan 1962; Koger 1972b, 1972e). This is the stage when the diffusion of Cr in the bulk material dictates the overall corrosion rate (DeVan and Evans III 1962; Koger 1972e; Evans III, DeVan, and Watson 1961), which is generally low (Keiser 1977; Koger 1974). Void formation, characteristic of the Cr depletion mechanism, was observed for temperatures closer to 800 ºC (DeVan and Evans III 1962).

Inconel 600 has previously been studied by Manly et al. (1957) in FCL testing in molten fluoride salts and it was reported that it behaved satisfactorily. In a work conducted by Keiser (1977), it was suggested that it would not be deemed suitable as a "containment vessel material". It was found that there is a rapid attack for the first 15 h, followed by a relatively constant rate, exhibiting a linear behavior. Similar behavior has also been reported previously for the TCL experiments (Sridharan and Allen 2013). Furthermore, it was stressed that the wall temperature had a greater effect on the corrosion process than the bulk temperature. The attack increased ~50μm for every 25°C increase in the wall temperature for the range 840-930 °C. For this reason, the regions near the highest wall temperature corroded much faster. Another parameter that was studied was the hot-leg surface area to the overall area of the loop. This ratio defines the depth of attack in the hot region. If the salt gets saturated with Cr ions in the hot zone, the surface area to volume ratio will be the rate determining step of the corrosion process in the mass-transfer stage.

Type 304 SS has also been examined by Koger [1970] in $NaBF_4$-8 mole% NaF molten salt inside an Inconel 600 tube, but the use of this material was by accident and severe galvanic corrosion was observed, leading to extensive selective attack of the stainless steel. Susskind et al. (1960) examined type 347 austenitic SS in ternary eutectic NaCl-KCl-$MgCl_2$ molten salt in isothermal conditions at 520 ºC and for two different flow velocities, and they identified transgranular corrosion in both cases.

4. Data quality and Uncertainty

Assessing the quality and uncertainty of data in molten salt corrosion tests is a challenging task due to the absence of standardized testing methods. Multiple variables, including the type of corrosion test, capsule or crucible material, cover gas conditions, alloy type, salt type, purification methods, impurity levels in the salt, temperature, pressure, duration of experiments, and post-test analysis methods, contribute to the complexity of the problem.

Salt purity

Raiman and Lee [2018] performed a meta-analysis of molten salt corrosion data collected from literature between 1960 and 2016, which revealed that salt purity had the most significant impact on corrosion rates. Other factors, such as alloy type, salt type (chloride vs. fluoride), and type of experiment, had a less pronounced impact on corrosion rates. The crucial lesson from this study is that impurities in salts may mask the effects of other factors, such as alloy type, on corrosion rates. Furthermore, when the halide salts are not purified, there is a greater scatter in data which makes it difficult to determine true effects a particular salt may have on structural or functional materials. Hence, the corrosion data obtained from purified salts should have greater merit when considering compatibility of materials with molten salts.

5. Cost

It is difficult to estimate costs for the various types of molten salt corrosion tests, i.e. static, TCL and FCL, and those costs can vary greatly. Clearly static testing is less expensive than dynamic testing. The pumps and valves required for a FCL make it the highest cost followed by TCLs and other dynamic options [Koger 1972c]. A rough estimate would be $3-5m for a FCL, $100-200K for a TCL (depending on the salt and tubing material) and $5K per static capsule test including post-exposure characterization of the specimen. The TCL cost assumes that the infrastructure is in place for operation including a walk-in hood, vacuum system for leak checking and a glovebox to handle loading the salt. Williams [2006] provided estimates of salt costs with chloride salts being the least expensive. However, salt purification is expensive and salts containing Be require extra handling and safety costs.

Some of the factors needed for a cost comparison are summarized in Table 1. Current FCLs have a larger salt volume 72-120 L compared to 2.4 L in earlier FCLs. The FCL pump is usually custom made and for a full size thermal storage plant the pump might cost $1m [Lopes 2021]. Current TCLs expose 40 specimens per test compared to smaller numbers in earlier studies. Finally, it should be noted that FCLs are built to conduct a wider range of studies including thermal hydraulic experiments and corrosion is not usually the primary focus at that stage of the development process.

Estimates are not available for rocker or spinning tests as those experiments have not been conducted in many years. An extensive design, development and safety analysis would be needed to conduct those experiments today. Based on this historical assessment of dynamic molten salt testing, TCLs became the favored flowing test during the MSRE program. A thermosiphon would likely have a similar expense as a TCL. Since the skilled workforce and facilities (gloveboxes and walk-in enclosures including temperature and heat tape controllers) for operating five TCLs are currently available at ORNL, the least expensive option for conducting a flowing salt test is a TCL.

Table 1:Technical components and capabilities of representative static, TCL and FCL experimental setup

	Static test	*Thermal Convection Loop (TCL) - Microloop*	*ORNL Thermal Convection Loop (TCL)-FLiNaK*	*FASTR FCL facility for CSP applications – chloride salt*	*FCL facility for FHR applications – FLiNaK*
Indicative References	Pint et al. (2019) Raiman et al. (2022)	Kelleher et al. (2022)	Pint 2019, Raiman 2022, Robb 2022	Robb [2019, 2022]	Yoder [2010,2014]
Max. operating temperature or CL-HL temperature for a TCL (ºC)	550-1000	500-620	550-750	725	700
Type of salt	NaCl-KCl-$MgCl_2$, FLiNaK, FLiBe	NaCl-KCl- $MgCl_2$	NaCl-KCl- $MgCl_2$, FLiNaK, FLiBe	NaCl-KCl- $MgCl_2$	FLiNaK
Flow rate (kg/s) or velocity (cm/s)	N/A	2.4-2.9 cm/s	1-3 cm/s	3-7 kg/s	4.5 kg/s
Sample material	Many different materials	Many, but Alloy 600 is selected for comparison purposes with the rest	Alloy 316H, 600, C276, 740H, etc.	Salt wetted surfaces: C-276 Main heater and level probes: Alloy 600	Alloy 600
Pump head (MPa)	N/A	N/A	N/A	0.148	0.125
Capsule/ Loop volume (L)	0.04	0.0134	2.5	120	72
Amount of salt (kg)	0.02-0.05		5.5	200	
Number of specimens/ corrosion test	1	Entire loop	40	6	Aimed for measurements of heat transfer characteristics of the working salt
Dimensions	OD=25 mm Thickness=1.2mm Length= 100 mm	OD=6.4 mm Thickness=0.89mm	OD=26.7 mm Thickness=2.79mm	OD=60.33 mm Thickness=3.91mm	

References

Adamson, Jr., G. M., R.S. Crouse, and W. D. Manly. 1959. Interim report on corrosion by alkali-metal fluorides: Work to May 1, 1953 (No. ORNL-2337). Oak Ridge National Lab., Tenn.

G. M. Adamson, Jr., R. S. Crouse, W. D. Manly, "Interim Report on corrosion by Zirconium-Based Fluorides," Technical Report ORNL-2338, Oak Ridge National Laboratory, Oak Ridge, TN 1961.

Ambrosek, James Wallace. 2011. "Molten chloride salts for heat transfer in nuclear systems." PhD, University of Wisconsin-Madison (UMI 3471128).

Bakish, R, and F Kern. 1960. "Selective Corrosion of Inconel." *Corrosion* 16 (11):533t-534t.

Briant, R.C., J.H. Buck, and A.J. Miller. 1953a. Aircraft nuclear propulsion project, Quartely progress report for period ending March 10, 1953, Oak Ridge National Laboratory Report ORNL-1515, Oak Ridge, TN.

Briant, R.C., and A.J. Miller. 1953b. Aircraft nuclear propulsion project, quarterly progress report for period ending June 10, 1953 (No. ORNL-1556). Oak Ridge National Lab., Tenn.

Britsch, Karl, Mark Anderson, Paul Brooks, and Kumar Sridharan. 2019. "Natural circulation FLiBe loop overview." *International Journal of Heat and Mass Transfer* 134:970-983.

Busby, Jeremy, Lauren M Garrison, Lianshan Lin, Stephen S Raiman, Sam Sham, Chinthaka Silva, Hong Wang, R Iyengar, and G Tartal. 2019. Technical Gap Assessment for Materials and Component Integrity Issues for Molten Salt Reactors (ORNL/SPR-2019/1089). Oak Ridge National Lab.(ORNL), Oak Ridge, TN (United States).

Cooke, JW, and B Cox. 1973. Forced-convection heat-transfer measurements with a molten fluoride salt mixture flowing in a smooth tube (No. ORNL-TM-4079). Oak Ridge National Lab., Tenn.

Crowley, JL, WB McDonald, and DL Clark. 1963. "Design and operation of forced-circulation corrosion testing loops with molten salt," Oak Ridge National Laboratory Report TM-528, Oak Ridge, TN.

DeVan, JH, and RB Evans III. 1962. Corrosion behavior of reactor materials in fluoride salt mixtures," Oak Ridge National Laboratory Report TM-328, Oak Ridge, TN.

Desmon, Leland G, and Don R Mosher. 1951. Preliminary Study of Circulation in an Apparatus Suitable for Determining Corrosive Effects of Hot Flowing Liquids (No. NACA-RM-E51D12). NACA, Cleveland, OH

Evans III, RB, JH DeVan, and GM Watson. 1961. Self-diffusion of chromium in nickel-base alloys (No. ORNL-2982). Oak Ridge National Lab., Tenn.

Guo, Shaoqiang, Jinsuo Zhang, Wei Wu, and Wentao Zhou. 2018. "Corrosion in the molten fluoride and chloride salts and materials development for nuclear applications." *Progress in Materials Science* 97:448-487.

Huntley, WR, and PA Gnadt. 1973. Design and operation of a forced-circulation corrosion test facility (MSR-FCL-1) employing Hastelloy N alloy and sodium fluoroborate salt," Oak Ridge National Laboratory Report TM-3863, Oak Ridge, TN.

Huntley, WR, and MD Silverman. 1976. System design description of forced-convection molten-salt corrosion loops MSR-FCL-3 and MSR-FCL-4," Oak Ridge National Laboratory Report TM-5540, Oak Ridge, TN.

Ignat'ev, VV, AI Surenkov, IP Gnidoi, VI Fedulov, VS Uglov, AV Panov, VV Sagaradze, VG Subbotin, AD Toropov, and VK Afonichkin. 2006. "Investigation of the corrosion resistance of nickel-based alloys in fluoride melts." *Atomic Energy* 101:730-738.

Ignatiev, Victor, Aleksandr Surenkov, Ivan Gnidoi, Vladimir Fedulov, Vadim Uglov, Valery Afonichkin, Andrei Bovet, Vladimir Subbotin, Aleksandr Panov, and Andrei Toropov. 2008. "Compatibility of selected Ni-based alloys in molten Li, Na, Be/F salts with PuF_3 and tellurium additions." *Nuclear technology* 164 (1):130-142.

Ignatiev, Victor, and Alexandr Surenkov. 2013. "Alloys compatibility in molten salt fluorides: Kurchatov Institute related experience." *Journal of Nuclear Materials* 441 (1-3):592-603.

Jordan, W.H., S.J. Croner, R.I. Strough, A.J. Miller, and A.W. Savolainen. 1955. Aircraft nuclear propulsion project quarterly progress report for period ending December 10, 1954 (No. ORNL-1816). Oak Ridge National Lab., Tenn. .

Keiser, JR, DL Manning, and RE Clausing. 1976. "Corrosion resistance of some nickel-base alloys to molten fluoride salts containing UF_4 and Tellurium." *ECS Proceedings Volumes* 1976 (1):315.

Keiser, JR. 1977a. Compatibility studies of potential molten-salt breeder reactor materials in molten fluoride salts," Oak Ridge National Laboratory Report TM-5783, Oak Ridge, TN.

Keiser, JR, JH DeVan, and DL Manning. 1977b. Corrosion resistance of type 316 stainless steel to Li_2BeF_4 (No. ORNL-TM-5782). Oak Ridge National Lab, Tenn.

Keiser, JR, JH DeVan, and EJ Lawrence. 1979. "Compatibility of molten salts with type 316 stainless steel and lithium." *Journal of Nuclear Materials* 85:295-298.

Kelleher, Brian C, Sean F Gagnon, and Ivan G Mitchell. 2022. "Thermal gradient mass transport corrosion in NaCl-$MgCl_2$ and $MgCl_2$-NaCl-KCl molten salts." *Materials Today Communications* 33:104358.

Knosalla, Christian, Marius Lau, Lennart Schmies, Wolfgang Lippmann, and Antonio Hurtado. 2020. "Investigation on the Corrosion Behavior of Nickel-Base Alloys in Molten Chlorides for Sensible Heat Energy Applications." *Advanced Engineering Materials* 22 (7):2000099.

Koger, JW, and AP Litman. 1969. Compatibility of Hastelloy N and Croloy 9M with $NaBF_4$-NaF-KBF_4 (90-4-6 mol%) Fluoroborate Salt (No. ORNL-TM-2490). In *ORNL-TM-2490*: Oak Ridge National Lab, Tenn.

Koger, JW, and AP Litman. 1970. Catastrophic corrosion of type 304 stainless steel in a system circulating fused sodium fluoroborate (No. ORNL-TM-2741). Oak Ridge National Lab., Tenn.

Koger, JW. 1972a. Alloy compatibility with LiF-BeF_2 salts containing ThF_4 and UF_4 (No. ORNL-TM-4286). Oak Ridge National Lab., Tenn.

Koger, JW. 1972b. Corrosion and mass transfer characteristics of $NaBF_4$-NaF (92-8 mole %) in Hastelloy N (No. ORNL-TM-3866). Oak Ridge National Lab.

Koger, JW. 1972c. Effect of FeF_2 addition on mass transfer in a Hastelloy N: LiF-BeF_2-UF_4 thermal convection loop system (No. ORNL-TM-4188). Oak Ridge National Lab.

Koger, JW. 1972d. Evaluation of Hastelloy N alloys after nine years exposure to both a molten fluoride salt and air at temperatures from 700 to 560 ^oC (ORNL-TM-4189). Oak Ridge National Lab, Tenn.

Koger, JW. 1972e. A forced-circulation loop for corrosion studies: Hastelloy N compatibility with $NaBF_4$--NaF (92-8 mole%) (No. ORNL-TM-4221). Oak Ridge National Lab., Tenn.(USA).

Koger, J. W. 1973. "Fluoride Salt Corrosion and Mass-Transfer in High-Temperature Dynamic-Systems." *Corrosion* 29 (3):115-122. doi: Doi 10.5006/0010-9312-29.3.115.

Koger, JW. 1974. "Corrosion product deposition in molten fluoride salt systems." *Corrosion* 30 (4):125-130.

Kondo, Masatoshi, Takuya Nagasaka, Valentyn Tsisar, Akio Sagara, Takeo Muroga, Takashi Watanabe, Tomoko Oshima, Yukihiro Yokoyama, Hiroshi Miyamoto, and Eiji Nakamura. 2010. "Corrosion of reduced activation ferritic martensitic steel JLF-1 in purified Flinak at static and flowing conditions." *Fusion engineering and design* 85 (7-9):1430-1436.

Lopes, Telma, Thomas Fasquelle, and Hugo G Silva. 2021. "Pressure drops, heat transfer coefficient, costs and power block design for direct storage parabolic trough power plants running molten salts." Renewable Energy 163:530-543.

Ma, Lina, Cancan Zhang, Yuting Wu, and Yuanwei Lu. 2022. "Comparative review of different influence factors on molten salt corrosion characteristics for thermal energy storage." *Solar Energy Materials and Solar Cells* 235:111485.

MacPherson, HG. 1960a. Molten-salt reactor program quarterly progress report for period ending July 31, 1960 (No. ORNL-3014). Oak Ridge National Lab., Tenn.

MacPherson, HG. 1960b. Molten-Salt Reactor Program Quarterly Progress Report for Period Ending October 31, 1959 (No. ORNL-2890). Oak Ridge National Lab., Tenn.

Manly, W. D., Jr. Adamson, G. M., J. H. Coobs, J. H. DeVan, D. A. Douglas, E. E. Hoffman, and P. Patriarca. 1957. Aircraft reactor experiment - metallurgical aspects (No. ORNL-2349). Oak Ridge National Lab., Tenn.

Manly, W.D., J.W. Allen, W.H. Cook, J.H. DeVan, D.A. Douglas, H. Inoye, D.H. Jansen, P. Patriarca, T.K. Roche, G.M. Slaughter, A. Taboada, and G.M. Tolson. 1958. "Construction materials for molten-salt reactors." In *Fluid-Fueled Reactors*, 595-625. Addison-Wesley.

McCoy, HE, and B McNabb. 1972. Intergranular Cracking of INOR-8 in the MSRE (No. ORNL-4829). Oak Ridge National Lab, Tenn.

Nagasaka, T, M Kondo, T Muroga, N Noda, A Sagara, O Motojima, A Suzuki, and T Terai. 2008. Progress in Flibe corrosion study toward material research loop and advanced liquid breeder blanket (IAEA-CN-165/FT/P2-4). National Institute for Fusion Science, Japan.

Olson, Luke C, James W Ambrosek, Kumar Sridharan, Mark H Anderson, and Todd R Allen. 2009. "Materials corrosion in molten LiF–NaF–KF salt." *Journal of Fluorine Chemistry* 130 (1):67-73.

Pint, Bruce A, Jake W McMurray, Adam W Willoughby, J Matthew Kurley, Samuel R Pearson, Michael J Lance, Donovan N Leonard, Harry M Meyer, Jiheon Jun, and Stephen S Raiman. 2019. "Re-establishing the paradigm for evaluating halide salt compatibility to study commercial chloride salts at 600 C–800 C." *Materials and Corrosion* 70 (8):1439-1449.

Pint, Bruce A, J Matthew Kurley, and Dino Sulejmanovic. 2022a, "Performance of alloy 600 in flowing commercial Cl salt at 600-750 C." AIP Conference Proceedings.

Pint, B. A., C. G. Parker, Y.-F. Su, D. Sulejmanovic, M. J. Lance and R. Pillai, 2022b, "Assessing Stainless Steel Compatibility in Flowing Fluoride Salts," in Proceedings of the 20th International Conference on Environmental Degradation of Materials in Nuclear Systems, paper ED2021-18337.

B. A. Pint, D. Sulejmanovic, R. Pillai and Y.-F. Su, "Evaluating Static Isothermal Molten Salt Compatibility with Structural Alloys," NRC Report, in press, 2023.

Raiman, S. S., and S. Lee. 2018. "Aggregation and data analysis of corrosion studies in molten chloride and fluoride salts." *Journal of Nuclear Materials* 511:523-535. doi: 10.1016/j.jnucmat.2018.07.036.

Raiman, Stephen S. Sulejmanovic, Dino, J. Matthew Lee Kurley, JoJo , Cory G. Parker, and Bruce A. Pint. 2021. Technical Assessment of Materials Compatibility in Molten Salt Reactors (TLR-RES/DE/CIB-CMB-2021-03). Oak Ridge National Lab., Tenn.

Raiman, Stephen S, J Matthew Kurley, Dino Sulejmanovic, Adam Willoughby, Scott Nelson, Keyou Mao, Chad M Parish, M Scott Greenwood, and Bruce A Pint. 2022. "Corrosion of 316H stainless steel in flowing FLiNaK salt." *Journal of Nuclear Materials* 561:153551.

Richardson, L. S., D. C . Vreeland and W. D. Manly, 1952, "Corrosion by Molten Fluorides, Oak Ridge National Laboratory Report ORNL-1491, Oak Ridge TN.

Robb, Kevin, Seth Baird, and Padhraic L Mulligan. 2020. Design Overview of the Facility to Alleviate Salt Technology Risks (FASTR). Oak Ridge National Lab.(ORNL), Oak Ridge, TN (United States).

Robb, Kevin, Ethan Kappes, and Padhraic L Mulligan. 2022. Facility to Alleviate Salt Technology Risks (FASTR): Design Report (No. ORNL/TM-2022/2803). Oak Ridge National Lab.(ORNL), Oak Ridge, TN.

Robb, Kevin R, Padhraic L Mulligan, Graydon L Yoder Jr, Kurt Smith, and Jordan Massengale. 2019. Facility to Alleviate Salt Technology Risks (FASTR): Preliminary Design Report with Failure Modes and Effects Analysis. Oak Ridge National Lab.(ORNL), Oak Ridge, TN (United States).

Rosenthal, M.W., R.B. Briggs, and P.N. Haubenreich. 1972. Molten-Salt Reactor Program: Semiannual Progress Report for Period Ending August 31, 1971 (No. ORNL-4728). Oak Ridge National Lab, Tenn.

Sabharwall, Piyush, Matt Ebner, Manohar Sohal, Phil Sharpe, Mark Anderson, Kumar Sridharan, James Ambrosek, Luke Olson, and Paul Brooks. 2010. Molten Salts for High Temperature Reactors: University of Wisconsin Molten Salt Corrosion and Flow Loop Experiments--Issues Identified and Path Forward (No. INL/EXT-10-18090). Idaho National Lab.(INL), Idaho Falls, ID (United States).

Silverman, MD, WR Huntley, and HE Robertson. 1976. Heat transfer measurements in a forced convection loop with two molten-fluoride salts: LiF-BeF_2-ThF_2-UF_4 and eutectic $NaBF_4$-NaF (No. ORNL-TM-5335). Oak Ridge National Lab.

Sohal, Manohar S, Piyush Sabharwall, Pattrick Calderoni, Alan K Wertsching, and S Brandon Grover. 2010. Conceptual design of forced convection molten salt heat transfer testing loop (INL-EXT-10-19908). Idaho National Lab.(INL), Idaho Falls, ID (United States).

Sridharan, K, and TR Allen. 2013. "Corrosion in molten salts." In *Molten salts chemistry*, 241-267. Elsevier.

Sridharan, Kumar, Mark Anderson, Michael Corradini, Todd Allen, Luke Olson, James Ambrosek, and Daniel Ludwig. 2008. Molten salt heat transport loop: materials corrosion and heat transfer phenomena (Project No.: 04-154). University of Wisconsin, Madison.

Susskind, H, FB Hill, L Green, S Kalish, LE Kukacka, WE McNulty, and E Wirsing Jr. 1960. Corrosion studies for a fused salt-liquid metal extraction process for the liquid metal fuel reactor (BNL 585, T-146). Brookhaven National Lab., Upton, NY.

Tavakoli Mehrabadi, B. A., J. W.Weidner, B. Garcia-Diaz, M. Martinez-Rodriguez, L. Olson and S. Shimpalee, 2016, “Multidimensional Modeling of Nickel Alloy Corrosion inside High Temperature Molten Salt Systems,” *Journal of The Electrochemical Society*, 163:C830-C838.

Tavakoli Mehrabadi, B. A., J. W.Weidner, B. Garcia-Diaz, M. Martinez-Rodriguez, L. Olson and S. Shimpalee, 2017, “Modeling the Effect of Cathodic Protection on Superalloys Inside High Temperature Molten Salt Systems,” *Journal of The Electrochemical Society*, 164:C171-C179.

Vreeland, D. C., E. E. Hoffman and W. D. Manly, 1953, “Corrosion Tests for Liquid Metals, Fused Salts at High Temperatures,” *Nucleonics* 11(11):36-39.

Wang, Yanli, Chaoliu Zeng, and Weihua Li. 2018. "The influence of temperature gradient on the corrosion of materials in molten fluorides." *Corrosion Science* 136:180-187.

Williams, D, D Wilson, J Keiser, L Toth, and J Caja. 2003. "Coolant/material interactions in advanced reactor systems, research on molten fluorides as high temperature heat transfer agents." American Nuclear Society Winter Meeting, New orleans, LA, November 20, 2003.

Williams, David F, Louis M Toth, and Kevin T Clarno. 2006. *Assessment of Candidate Molten Salt Coolants for the Advanced High Temperature Reactor (AHTR)*: United States. Department of Energy.

Yang, Xinmei, Huajian Liu, Bingchuan Chen, Min Ge, Yuan Qian, and Jianqiang Wang. 2022. "Corrosion behavior of GH3535 alloy in molten LiF–BeF_2 salt." *Corrosion Science* 199:110168.

Yoder, G, Dane F Wilson, Fred J Peretz, John B Wilgen, GR Romannski, Roger A Kisner, David Eugene Holcomb, Dennis Wayne Heatherly, and Adam M Aaron. 2010. "Development of a forced-convection liquid-fluoride-salt test loop (Paper 197)." Proceedings of HTR, Prague, Czech Republic, October 18–20, 2010.

Yoder Jr, Graydon L, Adam Aaron, Burns Cunningham, David Fugate, David Holcomb, Roger Kisner, Fred Peretz, Kevin Robb, John Wilgen, and Dane Wilson. 2014. "An experimental test facility to support development of the fluoride-salt-cooled high-temperature reactor." Annals of Nuclear Energy 64:511-517.